

# GasHisSDB: A New Gastric Histopathology Image Dataset for Computer Aided Diagnosis of Gastric Cancer

Weiming Hu<sup>a</sup>, Chen Li<sup>a,\*</sup>, Xiaoyan Li<sup>b</sup>, Md Mamanur Rahaman<sup>a</sup>, Jiquan Ma<sup>c</sup>, Yong Zhang<sup>b</sup>, Haoyuan Chen<sup>a</sup>, Wanli Liu<sup>a</sup>, Changhao Sun<sup>a</sup>, Yudong Yao<sup>d</sup>, Hongzan Sun<sup>e</sup> and Marcin Grzegorzek<sup>f</sup>

<sup>a</sup>*Microscopic Image and Medical Image Analysis Group, MBIE College, Northeastern University, 110169, Shenyang, PR China*

<sup>b</sup>*Department of Pathology, Cancer Hospital, China Medical University, Liaoning Cancer Hospital and Institute, Shenyang 110042, PR China*

<sup>c</sup>*Department of Computer Science and Technology, Heilongjiang University, Harbin, Heilongjiang, 150080, China*

<sup>d</sup>*Department of Electrical and Computer Engineering, Stevens Institute of Technology, Hoboken, NJ 07030, USA*

<sup>e</sup>*Department of Radiology, Shengjing Hospital, China Medical University, Shenyang, 110122, China*

<sup>f</sup>*Institute of Medical Informatics, University of Luebeck, Luebeck, Germany*

## ARTICLE INFO

### Keywords:

Gastric Histopathology

Sub-size Image

Database

Image classification

## ABSTRACT

Gastric cancer has turned out to be the fifth most common cancer globally, and early detection of gastric cancer is essential to save lives. Histopathological examination of gastric cancer is the gold standard for the diagnosis of gastric cancer. However, computer-aided diagnostic techniques are challenging to evaluate due to the scarcity of publicly available gastric histopathology image datasets. In this paper, a noble publicly available Gastric Histopathology Sub-size Image Database (GasHisSDB) is published to identify classifiers' performance. Specifically, two types of data are included: normal and abnormal, with a total of 245,196 tissue case images. This study also performed extensive experiments using traditional machine learning and deep learning methods to prove that the methods of different periods have discrepancies on GasHisSDB. To the best of our knowledge, it is the first publicly available gastric cancer histopathology dataset containing a large number of images for weakly supervised learning. We believe that GasHisSDB can attract researchers to explore new algorithms for the automated diagnosis of gastric cancer, which can help physicians and patients in the clinical setting. GasHisSDB is available at the URL: <https://gitee.com/neuhwm/GasHisSDB.git>

## 1. Introduction

Gastric cancer is a common type of malignant tumor with a relatively poor prognosis and presents a severe threat to global health [1]. According to the recent Global Cancer Statistics, gastric cancer is the fifth commonly diagnosed cancer [2], and accountable for 18.0% of the total cancer deaths [2]. Histopathological examination of gastric cancer is a microscopic examination of paraffin sections made from tissues taken from suspected cancerous sections by experienced pathologists [3]. It is the gold standard for gastric cancer diagnosis and an essential requirement before treatment initiation [1].

Hematoxylin and Eosin (H&E) staining is a commonly used staining method in paraffin section technology to demonstrate nucleus and cytoplasmic inclusions in clinical specimens and highlight the delicate structures of cells and tissues [4, 5, 6]. Firstly, the pathological segment is observed with naked eyes to observe whether the section is qualified or not to find the lesion roughly. Then, the use of a low magnification microscope to observe and diagnose. Finally, if doctors want to observe the fine structure of the lesion more clearly, they can move it to the center of the visual fields, switch to a high-power microscope for the analysis [7]. It can be seen that there are the following problems in the process of observing H&E staining sections of gastric cancer: the diagnosis results of medical doctors are subjective and

hard to be quantitative described, their workload is heavy, and working hours are long, it is easy for doctors to omit section information, and it is inconvenient to use big data technology. Therefore, there is an urgent need for more efficient solutions to related problems.

With the rapid development of computer vision technology, especially the emergence of medical image classification, it is possible to examine every electron microscopic photo quickly and efficiently. Thus, it brings an opportunity to solve the problems related to the diagnosis of gastric cancer [8, 9, 10]. Especially, image classification plays an important role in computer-aided diagnosis. In the field of distinguishing benign or malignant tumors, distinguishing the differentiation stage of tumors and distinguishing the subtype of cancer, the results of image classification methods can be used as an important reference for clinicians in diagnostic practice. Furthermore, with the development of medical image classification technology, the main purpose of this technology is to achieve high accuracy and have the high anti-interference ability [11, 12]. Although the mainstream trend is to scan the whole-slide images for analysis, the actual work often encounters the actual situation of computer performance shortage, where the whole-slide images are usually cropped into many sub-size images for analysis. To this end, we need a Sub-size Image Database to test the anti-interference ability of various medical image classification techniques [13].

This paper introduces a noble publicly available Gastric Histopathology Sub-size Image Database (GasHisSDB)

\*Corresponding author

 lichen201096@hotmail.com (C. Li)

, consisting of 245196 sub-size pathological images of gastric cancer and contains three sub-size labels. Furthermore, each image in this database calculates three different features. Moreover, the evaluation results of different classification schemes based on features and images, using machine learning and deep learning methods, are presented to show each classifier's discrimination ability.

The main contributions of this paper are as follows:

- Development of a Gastric Histopathology Subsize Image Database based on open-source databases, in which several experts participated in the production of the database.
- Demonstrate that GasHisSDB can be used to differentiate the performance of classifiers including traditional machine learning classifiers and deep learning classifiers.
- This Gastric Histopathology Subsize Image Database is published as open source for non-commercial purposes.

## 2. Related work

In the field of classical machine learning methods for gastric cancer image classification, a commonly used open-source database is introduced in [14]. This dataset consists of 11 Human Epidermal GrowthFactor Receptor 2 (HER2) and H&E stained Whole-Slide Images (WSI) at a magnification of 40×, annotated by ten pathologists, taken from surgical sections of patients with different gastric cancers [15]. In classical machine learning classification studies, this dataset is often pre-processed, including operations such as semi-automatic registration and conversion of HER2 WSI to H&E stained WSI [16]. Another commonly used open source database is the public database used in this paper [17], which contains 560 abnormal images and 140 normal images. Studies often pre-process this database, including random cuts, geometric transformations [18].

Meanwhile, some gastric cancer image classification studies use proprietary databases, such as the study using stomach molecular images taken from Pathology Department of the Medicine Faculty in the Firat University [19]. In the study, the size of these images is 2592×1944. 180 images are taken, of which 60 are normal, 60 are benign, and 60 are malignant.

The dataset in [14] is also public in the field of deep learning classification of gastric cancer images. In [20], this dataset is pre-processed with overlapping by a factor of 0.3, and affine transformations such as rotations with 10-degree intervals, reflection, rotation after reflection and shear by a factor of 0.1. After a further 512×512 cropping, this study yielded a total of 231000 initial data. In the field of deep learning classification, studies are using the same base database as [21]. In this study, the image pre-processing operation is to crop the whole image into 224×224 patches, obtaining 8992 abnormal patches and 14000 normal patches.

There are also deep learning studies of gastric cancer image classification using proprietary databases, as follows. A

new large Whole Slide Gastric Image dataset (WSGI) is constructed by collaborating with The Sixth Affiliated Hospital of Sun Yat-sen University in [22]. The WSGI dataset consists of 608 complete slide images with a magnification of 40×. The labels of WSGI include three categories: normal, dysplasia, and cancer. The dataset used in [23] contains 410 pathological images of gastric cancer of size 2048×2048 and 210 images of normal tissue of the same size. This study re-arrange and crop this dataset to 256×256 yielding 5905 training images and 655 test images. The deep learning model in the study of [24] is trained with 2123 pixel-level annotated H&E stained digital slides from 1500 patients, which include 958 surgical specimens (908 malignancies) and 542 biopsies (102 malignancies) with diverse tumor subtypes. Testing is then performed on a multicenter dataset, which included 355 cases (595 slides) from Peking Union Medical College Hospital and 541 cases (987 slides) from Cancer Hospital of Chinese Academy of Medical Sciences. In [25], a histopathological image dataset is obtained from gastroscopic biopsy specimens of 94 cases at Gyeongsang National University Changwon Hospital (Changwon, Korea). Then all 94 WSIs are manually categorized into four groups: 13 well-differentiated, 11 moderately-differentiated, 20 poorly-differentiated adenocarcinoma and 50 poorly cohesive carcinoma. And poorly cohesive carcinoma include 20 signet-ring cell features and 30 normal gastric mucosa.

Table. 1 summarizes existing studies and their use dataset for gastric histopathological image classification methods.

The databases proposed in the above papers include large size images and are in small quantities. Data augmentation operations are often performed on the databases to expect better classification performance of the classifiers. The source database utilized in this paper also has the aforementioned problems. Therefore, this study makes full use of the already existing resources and complements the shortcomings of the original database functionality to make it more comprehensive.

## 3. GasHisSDB

### 3.1. Database overview

GasHisSDB contains 245,196 sub-size images in two categories, including 97,076 abnormal images and 148,120 normal images. The details of the applied datasets are introduced as follows.

#### Gastric Histopathology Sub-size Image Database:

##### 1. Data source:

Stage 1: Four pathologists from Longhua Hospital Shanghai University of Traditional Chinese Medicine provide 600 images of gastric cancer pathology images of size 2048×2048 and give tissue-level labels for a strongly supervised learning process [17, 21, 26].

Stage 2: Based on stage 1, five biomedical researchers from Northeastern University prepare 245196 sub-sized gastric cancer pathology images for weakly supervised learning, and two experienced pathologists from Liaon-

**Table 1**  
Data usage in image classification of gastric cancer.

Aim	Year	Reference	Team	Categorization	Amount
Machine learning	2015	[14]	Sharma et al.	HER2+ tumor/HER2- tumor/Non-tumor	11
	2015	[16]	Sharma et al.	HER2+ tumor/HER2- tumor/Non-tumor	11
	2017	[18]	Liu et al.	Abnormal/Normal	560/140
	2018	[19]	Korkmaz et al.	Normal/Benign/Malignant	60/60/60
Deep learning	2017	[20]	Sharma et al.	HER2+ tumor/HER2- tumor/Non-tumor	11
	2018	[21]	Li et al.	Abnormal/Normal	560/140
	2019	[22]	Wang et al.	Normal/Dysplasia/Cancer	117/172/319
	2020	[23]	Zhu et al.	Cancer/Normal	410/210
	2020	[24]	Song et al.	Malignancy/Normal	1010/490
	2020	[25]	Kosaraju et al.	Well-differentiated/Moderately-differentiated/poorly-differentiated adenocarcinoma/poorly cohesive carcinoma	13/11/20/50

ing Cancer Hospital and Institute perform the calibration.

2. Preparation rules: According to the existing method of making the database [27, 28], the preparation rules of this database is as follows:

Rule 1: Three sizes (160 × 160, 120 × 120, 80 × 80 pixels) of normal pathological sections are cropped directly. And, it is necessary to select the cancerous region as the region of interest when dealing with abnormal pathological sections.

Rule 2: The region of interest of the pathological section and the ground truth is cropped simultaneously. This work can be used to filter out images with very few cancerous areas.

Rule 3: In order to reduce the correlation among sub-size images from the same original images, each one is rotated randomly, and the image order of the whole database is scrambled.

The data preparation workflow of GasHisSDB is shown in Figure. 1.

3. Staining: H&E staining (See section 3.2.3 for details).

4. Magnification: 20×.

5. Microscope: Nikon (Japan) and Olympus (Japan).

6. Acquisition software: NewUsbCamera.

7. Sub-database and image sizes:

Sub-database A: 160×160 pixels,

Sub-database B: 120×120 pixels,

Sub-database C: 80×80 pixels.

8. Scale: See Table. 2.

**Table 2**  
Dataset scale of GasHisSDB.

Sub-database name	Cropping size	Abnormal	Normal
Sub-database A	160 × 160 pixels	13,124	20,160
Sub-database B	120 × 120 pixels	24,801	40,460
Sub-database C	80 × 80 pixels	59,151	87,500
Total		97,076	148,120

9. Image format: ".png".

10. Image types:

Normal: No cancerous cells appeared in the section

(See section 3.2.1 for details); Abnormal: Cancerous cells appear in this section (See section 3.2.2 for details).

11. The research and preparation of GasHisSDB is approved by the Ethical Committee at Northeastern University.

### 3.2. Database description

#### 3.2.1. Normal image

Every normal image does not contain cancerous region. Each cell has no or very small atypia (Figure. 2 (a)). Moreover, the nuclei of the cells in the image have almost no mitosis and are regularly arranged in one layer (Figure. 2 (b)). Therefore, when observed under the optic microscope, if no cancellation of any cells and tissues is observed, and the characteristics of the normal image are satisfied, it can be judged that this is a normal image [29]. In making normal image data set, we directly crop the whole image because of the characteristics of normal images. The resulting images are shown in (a) (b) (c) in Figure. 3.

#### 3.2.2. Abnormal image

Each abnormal image contains gastric cancer. The general shape of gastric cancer is mostly ulcer type. As the disease progresses, cancer nests grow infiltrating from the mucosal layer to the muscle layer and serosal layer. It has a hard texture, and the section is often gray-white. When observing under a microscope, the cancer cells can be arranged in a nest, acinar, tubular, or cord shape, and the boundary with the stroma is generally clear (Figure. 2 (c)). However, when the cancer cells infiltrate into the stroma, the boundary between them is not clear (Figure. 2 (d)). Based on the above facts, when the cells are observed to form gland or adenoid structures with uneven size, different shapes, and irregular arrangement, it can be judged that the pathological image is abnormal. In the abnormal images, the cancerous cells are often irregularly arranged in many layers, and the nuclei have different sizes and division phenomena [1, 30, 31]. In the process of making the abnormal image dataset, we crop every cancerous region selected according to the original ground truth (GT) images. Then, the cropped images are

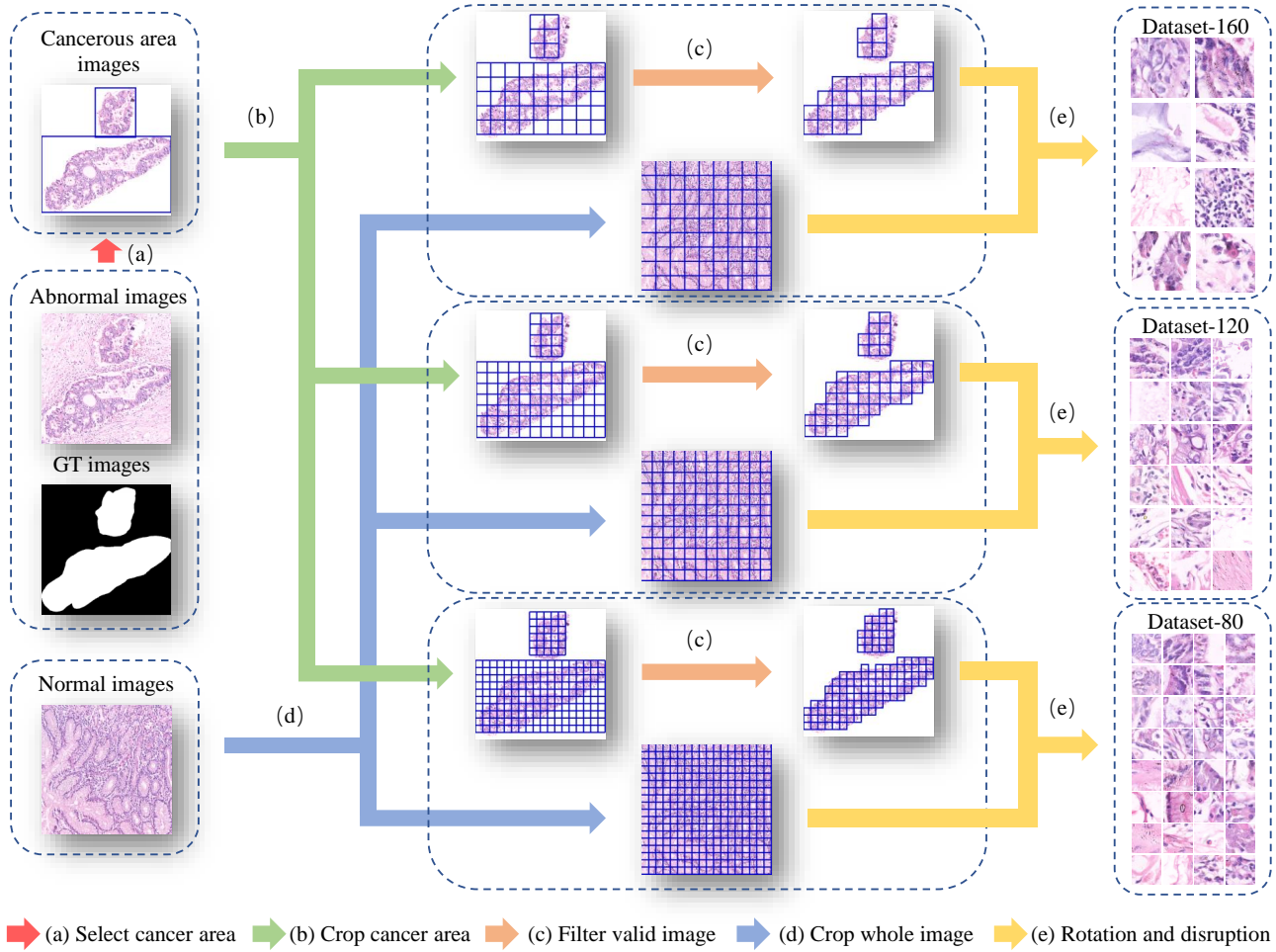


**Figure 1:** Data preparation workflow of GasHisSDB.

filtered based on the cancerous area (usually 50%) in the images. The resulted images are shown in Figure. 3 - (d)(e)(f).

### 3.2.3. Staining method

H&E staining method is one of the commonly used staining methods in paraffin section technology and is often the gold standard. The hematoxylin is alkaline and stains cell nuclei a purplish blue, and eosin is acidic and stains the extracellular matrix and cytoplasm pink, with other structures taking on different shades, hues, and combinations of these colors [5, 32]. Therefore, pathologists can easily distinguish the nuclear and cytoplasmic parts of cells. In addition, the overall staining pattern of staining shows the overall layout and distribution of the cells and provides a general overview of the structure of the tissue sample [33]. H&E staining method is the most basic and most widely used technical method in histology, embryology, pathology teaching and scientific research.

The pathological image after he staining has more pink and white areas in the normal image. Compared with the normal image, in the abnormal image, the purplish blue area

is more distributed and messy.

## 4. Evaluation of GasHisSDB

### 4.1. Methods of feature extraction

Extracting various virtual features of a database is the preparation for classification using a machine learning classifier. In this paper, we use three methods to extract the visual features of the database, including color histogram, local binary pattern (LBP), and gray level co-occurrence matrix (GLCM) features.

#### 4.1.1. Color histogram

Color histogram is the most commonly used method to describe the color characteristics of images. It can simply represent the global distribution of colors in an image, i.e., the proportion of different colors in the whole image. It is especially suitable for describing images that are difficult to segment automatically and images that do not need to consider the spatial location of objects [34, 35]. Its advantage is that it is not affected by image rotation, shift changes, and

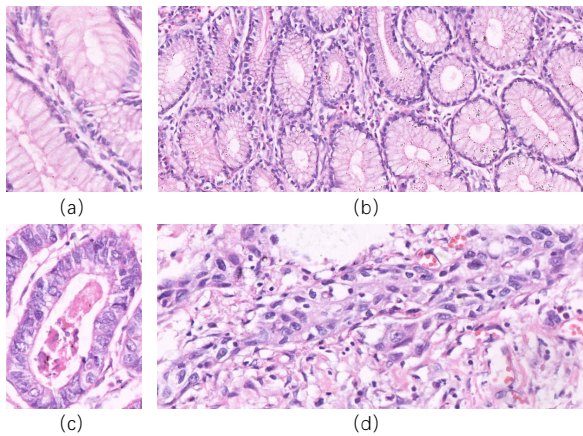


**Figure 2:** Example of Pathological images: (a)(b) Normal pathological images, (c) Non-invasive abnormal pathological image, (d) Invasive abnormal pathological image.

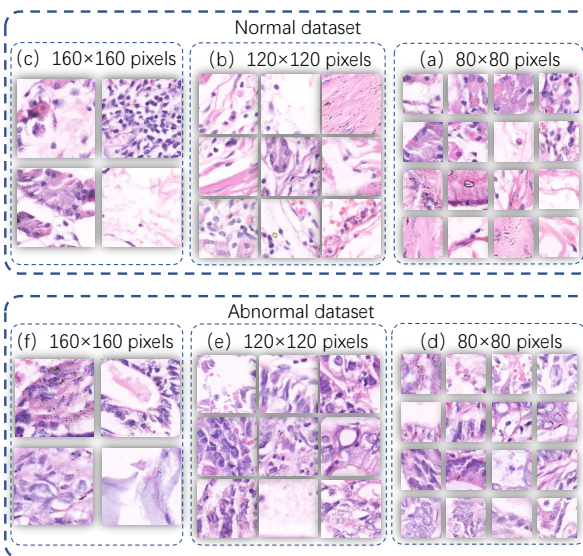


**Figure 3:** Example of GasHisSDB.

further normalization by image scale changes. The disadvantage is that it cannot describe the local distribution of colors in the image, each color's spatial location, and specific objects.

#### 4.1.2. Texture features

The texture is a visual feature that reflects homogeneity in an image. It reflects the organization and arrangement of surface structures with slow or periodic changes on the surface of an object. It is not based on the characteristics of pixels but needs to carry out the statistical calculation on the region containing multiple pixels [37]. The texture is represented by the gray distribution of pixels and their surrounding spatial neighbor, local texture information. Besides, global texture information is the degree of repetition

of local texture information. This paper uses two methods to describe texture features of GasHisSDB, which are Local Binary Patterns (LBP) and Gray-level Co-occurrence Matrix (GLCM).

LBP is an effective texture description operator that measures and extracts textural information local to an image with significant advantages such as grey level invariance and rotational invariance, and the feature is easy to compute. The value of LBP for each pixel is eight values within its eight-neighbor compared to its pixel. If the pixel value in the eight-neighbor is greater than or equal to the central pixel value, the position is labeled by 1, and 0 for otherwise, aligning them clockwise after eight comparisons yield a binary number of eight lengths, yielding LBP values [39].

The GLCM is defined by the joint probability density of the pixels at two locations. It not only reflects the distribution of brightness but also reflects the distribution of location between pixels with the same or near brightness. It is a second-order statistical feature about the change of image brightness. GLCM is the basis for defining a set of texture features [40, 41]. To more intuitively describe the texture state with a symbiotic matrix, some parameters reflecting the state of the matrix are derived from the symbiotic matrix, typically the following:

1. Contrast: Reflects the sharpness of the image and the depth of texture grooves.
2. Correlation: It measures the degree of similarity of spatial grayscale symbiosis matrix elements in a row or column directions.
3. Energy: It is the sum of squares of gray symbiosis matrix elements, so it is also called energy, which reflects the uniformity of gray distribution and texture thickness of the image.
4. Homogeneity: Returns a measure of the compactness of the diagonal distribution of elements in GLCM.

## 4.2. Classification

After the steps of feature extraction, two classical machine learning methods are used to classify GasHisSDB, including Random Forest (RF) and linear Support Vector Machine (linear SVM). Furthermore, three classical or novel deep learning methods are used to classify GasHisSDB, including VGG16, ResNet50 and ViT.

### 4.2.1. Classical machine learning methods

The machine learning method for classification interpreters whether the image is normal or not by its visual features. RF is a parallel ensemble learning method and an extended variant of Bagging. RF is based on a decision tree learner, which adds random attribute selection to the training process of the decision tree [46]. SVMs are classified into linear and non-linear according to the kernel functions. Linear SVM maps training examples to points in space to maximize the gap between the two categories. Then, the new examples are mapped to the same space and predicted to belong to a category based on which side of the gap they fall on.

#### 4.2.2. Deep learning methods

The concept of deep learning originates from the research of Artificial Neural Network [49], where a multi-layer perceptron with multiple hidden layers is a deep learning structure. Deep learning forms a more abstract high-level representation attribute category or feature by combining low-level features to discover distributed feature representations of data.

In 2014, the Visual Geometry Group and Google Deep-Mind developed a new deep convolutional neural network: VGG [50]. VGG is a *Convolutional Neural Network* (CNN) improved by AlexNet. Several forms of VGG models are released, and the most commonly used in the field of image classification is VGG16 one. In VGG16, three  $3 \times 3$  convolution kernels are used instead of  $7 \times 7$  convolution kernels, and two  $3 \times 3$  convolution kernels are used instead of  $5 \times 5$  convolution kernels. The main purpose of this structure is to ensure the same perceptual field conditions, enhance the depth of the network, and to a certain extent enhance the effect of the neural network.

In 2016, to solve the difficulty of training deep networks due to the disappearance of gradients, Kaiming He et al. proposed various forms of ResNet [52]. The most commonly used in the field of image classification is ResNet50. The ResNet50 team separately constructed a ResNet50 building block with "Shortcut Connection" and a down-sampling ResNet building block. A  $1 \times 1$  convolution operation is added to the main branch of the regional down-sampling building block.

In 2020, Alexey Dosovitskiy et al. proposed the ViT model [53] by using the transformer, which is very effective in the field of natural language processing. It also provides good results in the image classification domain and reduces the dependence on CNNs. ViT crops an image into small chunks and provides a sequence of linear embeddings of these chunks as input to the Transformer and trains the model in a supervised manner for image classification.

#### 4.3. Quantitative results of classical machine learning methods

In this paper, various classification experiments are conducted on the GasHisSDB database ( $160 \times 160$  pixels,  $120 \times 120$  pixels and  $80 \times 80$  pixels) to demonstrate that GasHisSDB can be used to discriminate the performance of classifiers. Table. 3 show the comparison results of the classical machine learning methods. All the classification comparison experiments use the same parameters. The number of trees in the RF is set to 10. The SVM kernel function uses a linear kernel.

Sub-database A has the largest sample size and the smallest number of samples. The color histogram is the extracted feature with the most feature items. According to Table. 3, the color histogram obtains the best classification accuracy in the classification results of different classifiers using three different features on Sub-database A in the RF, which is 85.99%. However, the linear SVM classifier performs poorly on color histogram features, less than 50%. As a comparison, the classification effect on LBP does not perform as well

as the color histogram, and the highest classification effect on RF is only 70.27%. And the classification effect of linear support vector machine on LBP is also less than 50%. GLCM contains the least amount of data among all features, with only four items per image. The classification results of RF on GLCM are similar to those on LBP, but the linear SVM has a significant improvement in classification accuracy reaching 66.50% on GLCM.

Sub-database B has more balanced sample size and sample number. Overall, there was only a slight change in the classification accuracy of Sub-database B compared to the classification results of Sub-database A. On Sub-database B, the best classification accuracy remained on the color histogram using RF classification, with a result of 86.08%. The RF is greater than 70% on all three features and performs consistently. Another classical machine learning classifier, linear SVM, achieves 66.66% on Sub-database B only on GLCM and performs poorly on the remaining features.

Sub-database C has the largest number of samples. In Sub-database C, RF changed its classification result on the color histogram to 83.27%, but still performed the best. Compared with the other two Sub-databases, the linear SVM classification results differed more reaching 60.81%. The classification accuracy of RF decreased slightly on LBP and GLCM, both below 70%. Linear SVM on LBP still underperforms. The linear SVM still underperforms on LBP, but performs the same on GLCM as on the other two sub-datasets.

#### 4.4. Quantitative results of deep learning methods

In this part, classical and novel deep learning methods are used to classify the Sub-database A, Sub-database B and Sub-database C of GasHisSDB. In a series of comparative experiments, the ratio of the training, validation and test sets to the three Sub-databases is split 4:4:2. Each model uses a learning rate of 0.00002, the batch size is set to 32, and the experiment is performed for 100 epochs, to observe the classification results of this database on different models. The results of the comparative experiment are shown in Table. 4.

In general, deep learning models are far superior to classical machine learning methods, and even the lowest ViT accuracy is still higher than the highest accuracy of classical machine learning methods. In Sub-database A, The accuracy of the VGG model is more than 95%, but it has the longest training time and the model size is much larger than other deep learning models. The accuracy of ResNet50 is slightly higher than that of VGG16, which is the highest value among all methods reaching 96.09%. Both the model size and training time of ResNet50 are better than VGG16. ViT is the latest model based on transformer structure. Its accuracy is at least 86.21%, but it is still higher than the classification accuracy of RF on the color histogram. Importantly, compared to ResNet, ViT achieves such accuracy in only 1/4 of the training time and 1/3 of the model size. Moreover, the accuracy curve still has an increasing trend and the loss function still has not fully converged.

Because there are more training samples, VGG16 is the

**Table 3**

Classification results of three image features using different classifiers in three sub-databases of GasHisSDB (In [%]). The bold text in the table indicates the highest value of the classification result for the same sub-database.

Sub-database	Features	Methods	Acc	Abnormal				Normal			
				Precision	Recall	Specificity	F1-score	Precision	Recall	Specificity	F1-score
Sub-database A (160×160 pixels)	Color histogram	RF	<b>85.99</b>	81.65	87.83	84.55	84.63	89.88	84.55	87.83	87.13
		linear SVM	41.12	33.92	35.96	45.16	34.91	47.40	45.16	35.96	46.25
		RF	70.27	62.16	62.84	75.10	62.50	75.64	75.10	62.84	75.37
	LBP	linear SVM	48.17	36.83	44.02	50.87	40.10	58.27	50.87	44.02	54.32
		RF	71.39	63.16	65.85	75.00	64.48	77.14	75.00	65.85	76.06
	GLCM	linear SVM	66.50	55.89	71.27	63.39	62.65	77.22	63.39	71.27	69.63
Sub-database B (120×120 pixels)	Color histogram	RF	<b>86.08</b>	80.36	83.87	87.43	82.08	89.84	87.43	83.87	88.62
		linear SVM	46.28	39.48	77.62	27.06	52.34	66.36	27.06	77.62	38.45
		RF	70.13	60.88	59.90	76.41	60.39	75.66	76.41	59.90	76.03
	LBP	linear SVM	46.21	29.70	30.40	55.89	30.05	56.71	55.89	30.40	56.30
		RF	71.15	61.42	64.72	75.09	63.03	77.64	75.09	64.72	76.34
	GLCM	linear SVM	66.66	55.02	67.30	66.28	60.54	76.78	66.28	67.30	71.14
Sub-database C (80×80 pixels)	Color histogram	RF	<b>83.27</b>	77.14	83.15	83.34	80.03	87.98	83.34	83.15	85.60
		linear SVM	60.81	50.86	83.58	45.41	63.24	80.36	45.41	83.58	58.03
		RF	68.16	60.13	62.49	71.98	61.29	73.95	71.98	62.49	72.95
	LBP	linear SVM	43.10	27.68	25.48	55.01	26.53	52.20	55.01	25.48	53.56
		RF	68.39	60.13	64.23	71.21	62.11	74.65	71.21	64.23	72.89
	GLCM	linear SVM	66.82	57.14	71.04	63.97	63.33	76.57	63.97	71.04	69.71

**Table 4**

Classification results of four deep learning classifiers on GasHisSDB (In [%]). The bold text in the table indicates the maximum value or the best index of the classification results of different categories.

Sub-database	Model	Quantity of epoch	Model size	best epoch	training time	Acc	Category	Precision	Recall	Specificity	F1-score
Sub-database A (160×160 pixels)	VGG16	100	268.16	100	13873	<b>95.90</b>	Abnormal	93.8	96.0	95.9	94.9
		100	83.12	84	10023	<b>96.09</b>	Normal	97.3	95.9	96.0	96.6
		100	31.17	97	2587	86.21	Abnormal	94.6	95.6	96.4	95.1
	ResNet50	100	31.17	97	2587	86.21	Normal	97.1	96.4	95.6	96.7
		400	31.17	399	10014	92.23	Abnormal	83.8	80.6	89.9	82.2
	ViT	400	31.17	399	10014	92.23	Normal	87.7	89.9	80.6	88.8
Sub-database B (120×120 pixels)	VGG16	100	268.16	100	26105	<b>96.47</b>	Abnormal	96.7	94.0	98.0	95.3
		100	83.12	94	19087	95.94	Normal	96.4	98.0	94.0	97.2
		100	31.17	100	4077	89.44	Abnormal	96.2	93.0	97.8	94.6
	ResNet50	100	31.17	100	4077	89.44	Normal	95.8	97.8	93.0	96.8
		500	31.17	496	20410	94.59	Abnormal	87.0	84.9	92.2	85.9
	ViT	500	31.17	496	20410	94.59	Normal	90.9	92.2	84.9	91.5
Sub-database C (80×80 pixels)	VGG16	100	268.16	90	62152	<b>96.12</b>	Abnormal	94.2	96.3	96.0	95.2
		100	83.12	97	41992	96.09	Normal	97.4	96.0	96.3	96.7
		100	31.17	89	8247	90.23	Abnormal	96.2	94.0	97.5	95.1
	ResNet50	100	31.17	89	8247	90.23	Normal	96.0	97.5	94.0	96.7
		500	31.17	496	41135	94.57	Abnormal	86.3	90.1	90.3	88.2
	ViT	500	31.17	496	41135	94.57	Normal	93.1	90.3	90.1	91.7

classifier with the highest accuracy in the classification results of the deep learning method of Sub-database B, which is 96.47%. The corresponding training time has also become twice that of Sub-database A. The accuracy of ResNet50 almost caught up with that of VGG16 with 95.94% accuracy. The accuracy of ViT also improved somewhat with the in-

crease in the amount of training data, reaching 89.44%.

Sub-database C is the Sub-database with the largest number of samples. The accuracy of the four classifiers has only slightly changed. The classification model with the highest accuracy rate is still 96.12% for VGG16. The lowest accuracy rate is still the ViT model with the least training time,

which is 90.23%. However, the training time of ViT in the Sub-database C has almost become 13.26% of the training time of VGG16 with the highest accuracy.

#### 4.5. Additional experiment

Since it is observed that the ViT did not fully converge in 100 epochs, a series of additional experiments are performed in this section. The experimental results are shown in the last item of each Sub-database in Table. 4. In the follow-up additional experiment of Sub-database A, under the same parameter conditions, the training time is controlled to be similar to that of ResNet with running 100 epochs, so ViT needed to run 400 epochs. This experiment achieved an accuracy of 92.23%. Moreover, as the amount of data increases, when the control training time is the same as ResNet50, the accuracy of the ViT model with Sub-database B and Sub-database C is increased to 94.59% and 94.57%. These image classification results have reached the general level of medical image classification, and the ViT model is excellent in terms of model size.

#### 4.6. discussion

This chapter compares the different classifier's classification results from the Linear Regression to Visual Transformer on the Sub-database A, Sub-database B and Sub-databases C of the GasHisSDB. Each method has a completely different classification performance on GasHisSDB. Classical machine learning methods have strict theoretical foundations, simple ideas, and excellent performance in some specific features and algorithms. However, deep learning methods are still far ahead of classical machine learning methods in terms of image classification accuracy and experimental workload. As a sub-size image database, GasHisSDB can be proved to have distinguishing in a variety of methods.

### 5. Conclusion and futures works

In this paper, a sub-size gastric histopathological image database is developed, namely GasHisSDB. GasHisSDB have three Sub-databases,  $160 \times 160$  pixels Sub-database,  $120 \times 120$  pixels Sub-database and  $80 \times 80$  pixels Sub-database. Each Sub-database contains two folders of normal images and abnormal images. Each folder contains cropped images that have been renamed and shuffled. GasHisSDB has the function of discriminating the performance of classifiers. This paper is divided into the following two parts for testing. For classical machine learning methods, this paper extracts five different features. Then test the classification performance of seven different classification methods on three sub-databases, and analyze the differences in the accuracy of each classifier. For deep learning methods, this paper tests three repeatedly proven CNN methods and ViT, which have only recently been used in the field of image classification. This paper focuses on the analysis of the four models from the accuracy rate, model size, training time and other indicators. In addition, this paper conducts additional experiments for training time to find the best classification performance of ViT on GasHisSDB. GasHisSDB demonstrates that the

performance in the image classification experiments in this paper is competent to test existing image classification methods.

The creation of the dataset means that more image classification methods can be used for this dataset. We will try newer image classification methods on the GasHisSDB to compare and analyze image classification methods and obtain better practical methods to contribute to medical progress.

### 6. Acknowledgements

This work is supported by the "National Natural Science Foundation of China" (No. 61806047) and the "Fundamental Research Funds for the Central Universities" (No. N2019003). We also thank Miss. Zixian Li and Mr. Guoxian Li for their important discussion in this work.

### References

- [1] Feng Hua Wang, L. Shen, J. Li, Zhi Wei Zhou, H. Liang, Xiao Tian Zhang, L. Tang, Y. Xin, J. Jin, and Yu Jing Zhang. The chinese society of clinical oncology (cscos): Clinical guidelines for the diagnosis and treatment of gastric cancer. *Cancer Communications*, 39(1), 2019.
- [2] Hyuna Sung, Jacques Ferlay, Rebecca L. Siegel, Mathieu Laversanne, Isabelle Soerjomataram, Ahmedin Jemal, and Freddie Bray. Global cancer statistics 2020: GLOBOCAN estimates of incidence and mortality worldwide for 36 cancers in 185 countries. *CA: A Cancer Journal for Clinicians*, 0(0):1–41, 2021.
- [3] Tom, Waddell, Marcel, Verheij, William, Allum, David, Cunningham, Andrés, and Cervantes. Gastric cancer†: Esmo—esso—estro clinical practice guidelines for diagnosis, treatment and follow-up. *Radiotherapy and Oncology*, 2014.
- [4] Jack Rose Rolf Zeller Andrew H Fischer, Kenneth A Jacobson. Hematoxylin and eosin staining of tissue and cell sections. *CSH protocols*, 2008.
- [5] John K C Chan. The wonderful colors of the hematoxylin-eosin stain in diagnostic surgical pathology. *Int J Surg Pathol*, 22(1):12–32, 2014.
- [6] Robert D Cardiff, Claramae H Miller, and Robert J Munn. Manual hematoxylin and eosin staining of mouse tissue sections. *Cold Spring Harbor protocols*, 2014(6):655–658, 2014.
- [7] Vinay Kumar, Abul K Abbas, and Jon C Aster. *Robbins basic pathology e-book*. Elsevier Health Sciences, 2017.
- [8] David Forsyth and Jean Ponce. Computer vision: A modern approach., 2011.
- [9] Andrianos Tsekrekos, Sönke Detlefsen, Robert Riddell, James Conner, Luca Mastracci, Kieran Sheahan, Jayant Shetye, Lars Lundell, and Michael Vieth. Histopathologic tumor regression grading in patients with gastric carcinoma submitted to neoadjuvant treatment: results of a delphi survey. *Human pathology*, 84:26–34, 2019.
- [10] Peng Jin, Xiaoyan Ji, Wenzhe Kang, Yang Li, Hao Liu, Fuhai Ma, Shuai Ma, Haitao Hu, Weikun Li, and Yantao Tian. Artificial intelligence in gastric cancer: A systematic review. *Journal of Cancer Research and Clinical Oncology*, pages 1–12, 2020.
- [11] E. Miranda, M. Aryuni, and E. Irawansyah. A survey of medical image classification techniques. In *2016 International Conference on Information Management and Technology (ICIMTech)*, pages 56–61, 2016.
- [12] Carlos Affonso, André Luis Debiaso Rossi, Fábio Henrique Antunes Vieira, André Carlos Ponce de Leon Ferreira, et al. Deep learning for biological image classification. *Expert Systems with Applications*, 85:114–122, 2017.
- [13] Hiral Kotadiya and Darshana Patel. Review of medical image classification techniques. In *Third International Congress on Information and Communication Technology*, pages 361–369. Springer, 2019.

[14] Harshita Sharma, Norman Zerbe, Daniel Heim, Stephan Wienert, Hans-Michael Behrens, Olaf Hellwich, and Peter Hufnagl. A multi-resolution approach for combining visual information using nuclei segmentation and classification in histopathological images. In *ViS-APP (3)*, pages 37–46, 2015.

[15] Hans-Michael Behrens, Viktoria S Warneke, Christine Böger, Nele Garbrecht, Eva Jüttner, Wolfram Klapper, Micaela Mathiak, Ilse Oschlies, Ursula Rudolph, Christiane Stuhlmann-Laeisz, et al. Reproducibility of her2/neu scoring in gastric cancer and assessment of the 10% cut-off rule. *Cancer medicine*, 4(2):235–244, 2015.

[16] Harshita Sharma, Norman Zerbe, Christine Böger, Stephan Wienert, Olaf Hellwich, and Peter Hufnagl. A comparative study of cell nuclei attributed relational graphs for knowledge description and categorization in histopathological gastric cancer whole slide images. In *2017 IEEE 30th International Symposium on Computer-Based Medical Systems (CBMS)*, pages 61–66. IEEE, 2017.

[17] Pathological section identification of ai challenge. <http://www.datadreams.org/race-data-3.html>, 2017.

[18] Bo Liu, Ming Zhang, Tongyu Guo, and Yuanzhi Cheng. Classification of gastric slices based on deep learning and sparse representation. In *2018 Chinese Control And Decision Conference (CCDC)*, pages 1825–1829. IEEE, 2018.

[19] Sevcan Aytaç Korkmaz and Hamidullah Binol. Classification of molecular structure images by using ann, rf, lbp, hog, and size reduction methods for early stomach cancer detection. *Journal of Molecular Structure*, 1156:255–263, 2018.

[20] Harshita Sharma, Norman Zerbe, Iris Klempert, Olaf Hellwich, and Peter Hufnagl. Deep convolutional neural networks for automatic classification of gastric carcinoma using whole slide images in digital histopathology. *Computerized Medical Imaging and Graphics*, 61:2–13, 2017.

[21] Yuxiang Li, Xuechen Li, Xinpeng Xie, and Linlin Shen. Deep learning based gastric cancer identification. In *2018 IEEE 15th International Symposium on Biomedical Imaging (ISBI 2018)*, pages 182–185. IEEE, 2018.

[22] Shujun Wang, Yaxi Zhu, Lequan Yu, Hao Chen, Huangjing Lin, Xiangbo Wan, Xinjuan Fan, and Pheng-Ann Heng. Rmdl: Recalibrated multi-instance deep learning for whole slide gastric image classification. *Medical image analysis*, 58:101549, 2019.

[23] Zhonghang Zhu, Xin Ding, Defu Zhang, and Liansheng Wang. Weakly-supervised balanced attention network for gastric pathology image localization and classification. In *2020 IEEE 17th International Symposium on Biomedical Imaging (ISBI)*, pages 1–4. IEEE, 2020.

[24] Zhigang Song, Shuangmei Zou, Weixun Zhou, Yong Huang, Liwei Shao, Jing Yuan, Xiangnan Gou, Wei Jin, Zhanbo Wang, Xin Chen, et al. Clinically applicable histopathological diagnosis system for gastric cancer detection using deep learning. *Nature communications*, 11(1):1–9, 2020.

[25] Sai Chandra Kosaraju, Jie Hao, Hyun Min Koh, and Mingon Kang. Deep-hipo: Multi-scale receptive field deep learning for histopathological image analysis. *Methods*, 179:3–13, 2020.

[26] Changhao Sun, Chen Li, Jinghua Zhang, Md Mamanur Rahaman, Shiliang Ai, Hao Chen, Frank Kulwa, Yixin Li, Xiaoyan Li, and Tao Jiang. Gastric histopathology image segmentation using a hierarchical conditional random field. *Biocybernetics and Biomedical Engineering*, 40(4):1535–1555, 2020.

[27] Chen Li, Hao Chen, Le Zhang, Ning Xu, Dan Xue, Zhijie Hu, He Ma, and Hongzan Sun. Cervical histopathology image classification using multilayer hidden conditional random fields and weakly supervised learning. *Ieee Access*, 7:90378–90397, 2019.

[28] Božidar Potočnik, Jurij Munda, Milan Reljić, Ksenija Rakić, Jure Knez, Veljko Vlasiavljević, Gašper Sedej, Boris Cigale, Aleš Holobar, and Damjan Zazula. Public database for validation of follicle detection algorithms on 3d ultrasound images of ovaries. *Computer Methods and Programs in Biomedicine*, 196:105621, 2020.

[29] Sharon W Weiss, John R Goldblum, and Andrew L Folpe. *Enzinger and Weiss's soft tissue tumors*. Elsevier Health Sciences, 2007.

[30] Japanese Gastric Cancer Association [jgca@koto.kpu-m.ac.jp](mailto:jgca@koto.kpu-m.ac.jp). Japanese classification of gastric carcinoma: 3rd english edition. *Gastric cancer*, 14:101–112, 2011.

[31] Tsunehiro Takahashi, Yoshiro Saikawa, and Yuko Kitagawa. Gastric cancer: current status of diagnosis and treatment. *Cancers*, 5(1):48–63, 2013.

[32] Alan Stevens. The haematoxylins. *Theory and practice of histological techniques*, 1990.

[33] D Wittekind. Traditional staining for routine diagnostic pathology including the role of tannic acid. 1. value and limitations of the hematoxylin-eosin stain. *Biotechnic & histochemistry*, 78(5):261–270, 2003.

[34] Theo Gevers, Joost Van De Weijer, and Harro Stokman. Color feature detection, 2006.

[35] Joost Van De Weijer and Cordelia Schmid. Coloring local feature extraction. In *European conference on computer vision*, pages 334–348. Springer, 2006.

[36] Ze Lu, Xudong Jiang, and Alex Kot. Color space construction by optimizing luminance and chrominance components for face recognition. *Pattern Recognition*, 83:456–468, 2018.

[37] Mona Sharma and Sameer Singh. Evaluation of texture methods for image analysis. In *The Seventh Australian and New Zealand Intelligent Information Systems Conference, 2001*, pages 117–121. IEEE, 2001.

[38] Yanwei Pang, Yuan Yuan, Xuelong Li, and Jing Pan. Efficient hog human detection. *Signal Processing*, 91(4):773–781, 2011.

[39] Shu-Ren Zhou and Jian-Ping Yin. Lbp texture feature based on haar characteristics. *Journal of Software*, 24(8):1909–1926, 2013.

[40] P Mohanaiah, P Sathyaranayana, and L GuruKumar. Image texture feature extraction using glcm approach. *International journal of scientific and research publications*, 3(5):1–5, 2013.

[41] HOU Qunqun, WANG Fei, and YAN Li. Extraction of color image texture feature based on gray-level co-occurrence matrix. *Remote Sensing for Land & Resources*, 25(4):26–32, 2013.

[42] Douglas C Montgomery, Elizabeth A Peck, and G Geoffrey Vining. *Introduction to linear regression analysis*. John Wiley & Sons, 2021.

[43] Leif E Peterson. K-nearest neighbor. *Scholarpedia*, 4(2):1883, 2009.

[44] Irina Rish et al. An empirical study of the naive bayes classifier. In *IJCAI 2001 workshop on empirical methods in artificial intelligence*, volume 3, pages 41–46, 2001.

[45] Daniel Berrar. Bayes' theorem and naive bayes classifier. *Encyclopedia of Bioinformatics and Computational Biology: ABC of Bioinformatics*; Elsevier Science Publisher: Amsterdam, The Netherlands, pages 403–412, 2018.

[46] Andy Liaw, Matthew Wiener, et al. Classification and regression by randomforest. *R news*, 2(3):18–22, 2002.

[47] William S Noble. What is a support vector machine? *Nature biotechnology*, 24(12):1565–1567, 2006.

[48] Shan Suthaharan. Support vector machine. In *Machine learning models and algorithms for big data classification*, pages 207–235. Springer, 2016.

[49] Mohamad H Hassoun et al. *Fundamentals of artificial neural networks*. MIT press, 1995.

[50] Karen Simonyan and Andrew Zisserman. Very deep convolutional networks for large-scale image recognition. *arXiv preprint arXiv:1409.1556*, 2014.

[51] Christian Szegedy, Vincent Vanhoucke, Sergey Ioffe, Jon Shlens, and Zbigniew Wojna. Rethinking the inception architecture for computer vision. In *Proceedings of the IEEE conference on computer vision and pattern recognition*, pages 2818–2826, 2016.

[52] Kaiming He, Xiangyu Zhang, Shaoqing Ren, and Jian Sun. Deep residual learning for image recognition. In *Proceedings of the IEEE conference on computer vision and pattern recognition*, pages 770–778, 2016.

[53] Alexey Dosovitskiy, Lucas Beyer, Alexander Kolesnikov, Dirk Weissenborn, Xiaohua Zhai, Thomas Unterthiner, Mostafa Dehghani, Matthias Minderer, Georg Heigold, Sylvain Gelly, et al. An image is worth 16x16 words: Transformers for image recognition at scale. *arXiv preprint arXiv:2010.11929*, 2020.